frontiers in Energy Research

ORIGINAL RESEARCH
published: 28 March 2022
doi: 10.3389/fenrg.2022.836456

Hydraulic Characteristics of Axial Flow Pump Device With Different Guide Vane Inlet Angles

Lei Xu[1], Hucheng Zhang[1], Chuan Wang[2,3], Dongtao Ji[1], Wei Shi[4], Weigang Lu[1] and Linguang Lu[1]*

[1]College of Hydraulic Science and Engineering, Yangzhou University, Yangzhou, China, [2]International Shipping Research Institute, GongQing Institute of Science and Technology, Jiujiang, China, [3]High-tech Key Laboratory of Agricultural Equipment and Intelligentization of Jiangsu Province, Jiangsu University, Zhenjiang, China, [4]Jiangsu Water Supply Co., Ltd. In Eastern Route of S-to-N Water Diversion Project, Nanjing, China

To improve the efficiency of low-head pump device in the large-discharge and low-head domain, the hydraulic characteristics of vertical axial flow pump devices with different guide vane inlet angles were studied using computational fluid dynamics (CFD) and model test methods. The $Q \sim H_{zz}$ and $Q \sim \eta_{zz}$ curves of the pump device were obtained for different impeller blade angles when the inlet angle adjustments of the guide vane were 0° and −12°. The resulting hydraulic performance was compared and analyzed. The results showed that the pump device efficiency under low-head and large-discharge conditions was improved when the guide vane inlet angle was rotated in the clockwise direction. The reason for the increased pump device efficiency was analyzed using CFD. When the guide vane inlet angle adjustments were 0° and −12° under low-head working conditions, the vortex in the guide vane was eliminated, the hydraulic loss of the guide vane decreased, and the energy performance of the pump improved. When the operational conditions of the pump device deviate from its high-efficiency zone due to limitations in the pump model or the motor itself, the application of these results could improve its hydraulic performance, which is of great significance to the design and application of low-head pump devices.

Keywords: axial-flow pump device, guide vane, inlet angle, hydraulic characteristics, numerical simulation, model test

OPEN ACCESS

Edited by:
Xiaojun Li,
Zhejiang Sci-Tech University, China

Reviewed by:
Kan Kan,
College of Energy and Electrical Engineering, China
Peijian Zhou,
China Jiliang University, China
Yu Chen,
Nanjing Institute of Technology (NJIT), China

****Correspondence:***
Lei Xu
leixu@yzu.edu.cn

Specialty section:
This article was submitted to Process and Energy Systems Engineering, a section of the journal Frontiers in Energy Research

Received: *15 December 2021*
Accepted: *24 January 2022*
Published: *28 March 2022*

Citation:
Xu L, Zhang H, Wang C, Ji D, Shi W, Lu W and Lu L (2022) Hydraulic Characteristics of Axial Flow Pump Device With Different Guide Vane Inlet Angles. Front. Energy Res. 10:836456. doi: 10.3389/fenrg.2022.836456

INTRODUCTION

Low-head pumping stations are widely used in fields such as water resource allocation, agriculture irrigation and drainage, urban drainage, and water environment improvement plans. The design heads of many of these pumping stations can be very low—that is, approximately 1.0 m (Qi et al., 2017; Yu et al., 2018). Affected by the pump model and motor, the pump devices used in these pumping stations often operate in low-head and large-discharge areas, which deviate from high-efficiency areas, resulting in the operational efficiency of the pumping stations being low (Wu et al., 2016).

The vertical axial flow pump device is arranged in the vertical direction, having the advantages of a simple structure, excellent heat dissipation, convenient installation and maintenance, and mature design and manufacture (Liu et al., 2008; Zhang et al., 2011); it is also widely applied in low-head pumping stations. It consists of an inlet conduit, impeller, guide vane, and outlet conduit, the hydraulic characteristics of the pump device being determined by these four components and their

mutual matching. For example, the guide vane is used to recycle the kinetic energy of the water flow, its hydraulic design impacting the hydraulic performance of the pump and pump device. With a guide vane installed in the pump, water flow from the impeller outlet with tangential velocity is partly eliminated, and the water flow energy is converted into pressure energy, the recyclable rotation kinetic energy of the flow using the guide vane accounting for 10–15.7% of the total energy of the impeller outlet (Tang and Wang, 2006; Li et al., 2009). Compared to an axial flow pump with no guide vane, the efficiency can be improved by 5% when a guide vane is installed in the pump (Hu et al., 2008). The design of the guide vane clearly influences the position of the high-efficiency area for the pump (Zhou and Xu, 2007). Previous studies have shown that the pump device efficiency and discharge with the guide vane were higher than those for a pump device with no guide vane under design working conditions (Feng et al., 2012). To improve the efficiency of the axial flow pump, the influence of the guide vane angle adjustments on the hydraulic performance of the axial flow pump has been studied; the results have shown that the water head and efficiency of the axial flow pump increase when the guide vane is adjusted from the off-design condition, the pump efficiency improving by a maximum of 2.16%, and the stable operating range broadening (Qian et al., 2010; Qian et al., 2013).

The vertical axial flow pump device used in extra-low-head pumping stations usually works in a large-discharge area deviating from the high-efficiency area of the pump device, with the inlet angle of the guide vane not matching the direction of water flow at the impeller outlet. Consequently, the pump device efficiency can be improved by adjusting the inlet angle of the guide vane. Another function of the guide vane is that it can be used to fix the guide bearing in its wheel hub so that only the inlet angle of the guide vane can be adjusted.

Computational fluid dynamics (CFD) has been widely used in studies of the axial flow pump (Kan et al., 2021a; Al-Obaidi, 2021), submersible pump (Patil et al., 2019; Wang et al., 2021), centrifugal pump (Gonzalez and Santolaria, 2006; Wang et al., 2020a), the intake of pumping stations (Zhou et al., 2021) and the pump device (Kan et al., 2017), and other aspects (Wang et al., 2020b; Tang et al., 2021; Zawistowski and Kleiber, 2021; Zhang et al., 2021; Zhu et al., 2021), providing a convenient and effective method for their design and performance optimization. This study focuses on the vertical axial flow pump device and examines the influence of adjusting the guide vane inlet angle on energy performance of the pump device using three-dimensional turbulence flow numerical simulations. The results of the study are verified using a pump device model test.

PUMP DEVICE AND METHODS

Parameters of Axial Flow Pump Device

Based on the parameters of a low-head pumping station, the influence of the guide vane inlet angle adjustment on energy performance of a vertical axial flow pump device was investigated. The parameters of the pumping station were as follows: the design head, maximum head, and minimum head were 1.08, 1.5, and 0.11 m respectively; the design discharge of one pump was 6.67 m^3/s; the TJ04-ZL-07 pump model, used in the pump test in the same test-bed as for the South-to-North Water Diversion Project, was chosen (Liu et al., 2006); the prototype pump impeller diameter (D_P) and prototype pump rotation speed (n_P) were 1,460 mm and 247 r/min, respectively, based on the principle that the prototype (nD) and the model (nD) were equal, the model pump impeller diameter (D_m) and model pump rotation speed (n_m) being 300 mm and 1,200 r/min, respectively. The performance curve of the pump selection for this pumping station is shown in **Figure 1**. It can be seen that the design operating point is in the large-discharge and low-head area and that the pump efficiency is low.

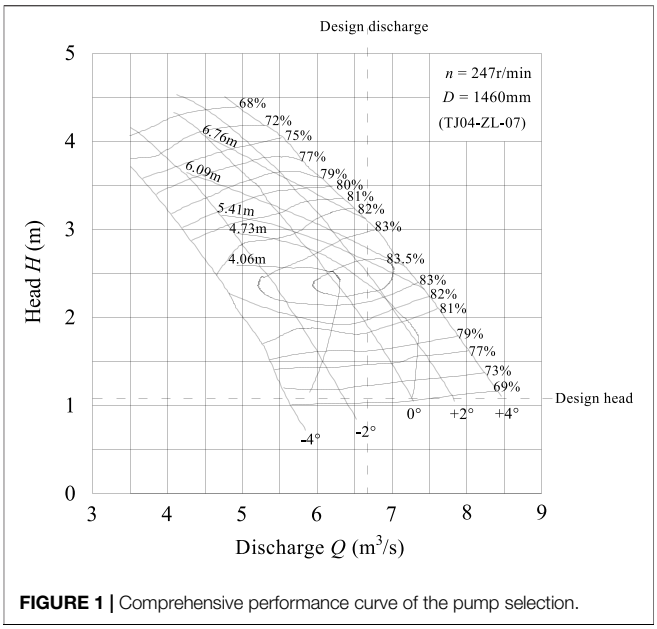

FIGURE 1 | Comprehensive performance curve of the pump selection.

The elbow inlet and siphon outlet conduits were adopted in the pumping station, a drawing of the vertical axial flow pump device model being shown in **Figure 2**.

Adjustment Scheme of Guide Vane Inlet Angle

In the vertical axial flow pump device, the guide vane inlet continues the water flow from the impeller; thus, the inlet shape line design needs to meet the requirement that the stream flows into the guide vane smoothly. The stream then flows into the outlet conduit from the guide vane. Therefore, the outlet shape line design needs to meet the requirement that it efficiently adjusts the flow direction. From a structural design point of view, a guide bearing is installed in the guide vane wheel hub. Thus, the guide vane needs to meet the requirement of securing the guide bearing block.

Based on the guide vane hydraulic design and structure requirements, the guide vane can be divided into three sections—that is, the inlet, middle, and outlet sections, as shown in **Figure 3**, where H is the total height of the guide vane and h is the inlet height of the guide vane. In this study, the

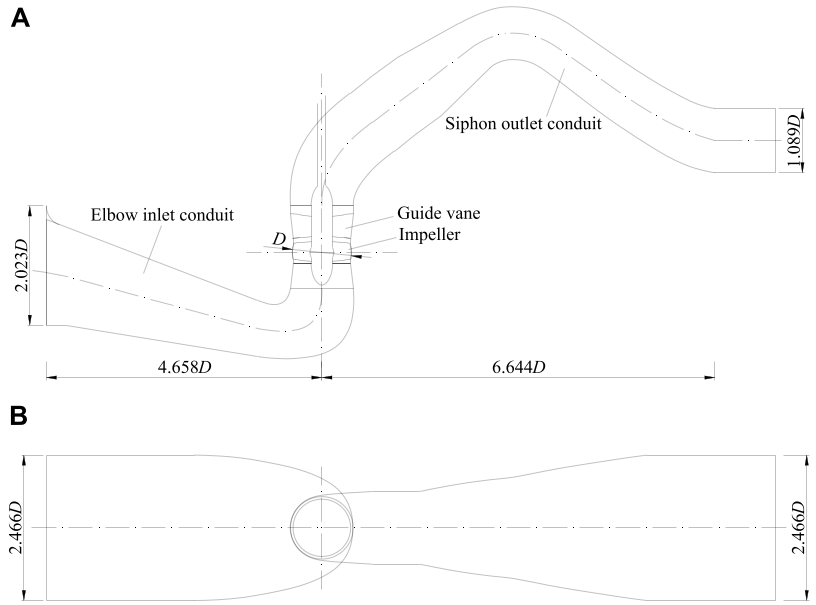

FIGURE 2 | Drawing of the vertical axial-flow pump device. **(A)** Elevation, **(B)** Plan.

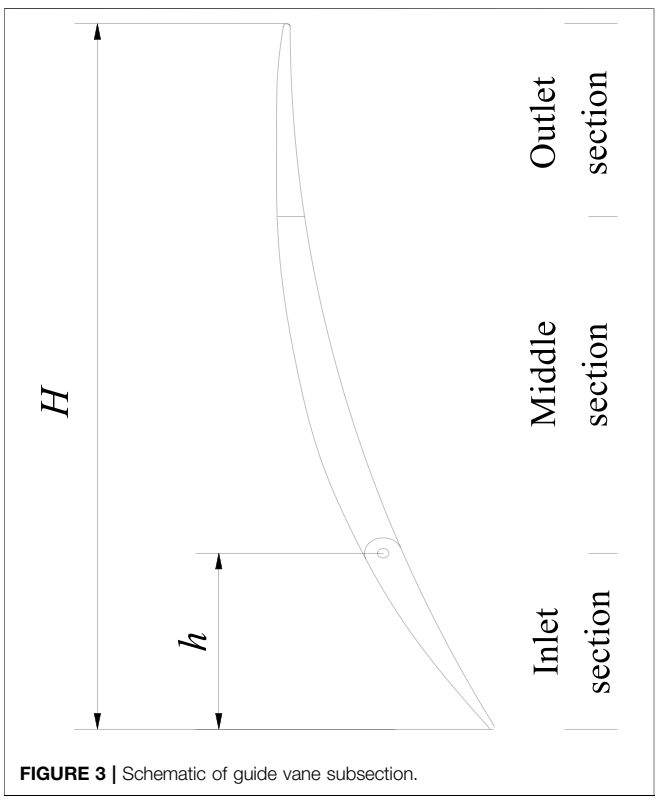

FIGURE 3 | Schematic of guide vane subsection.

middle and outlet sections were fixed, and only the angle of the inlet section could be adjusted. When the total height of guide vane (H) is a constant value, when the inlet height of the guide vane (h) is higher, the fixed length of the guide vane is reduced, adversely impacting the function of the fixed guide bearing block. Moreover, when h is lower, the influence of the guide vane adjustment on the hydraulic performance of the pump is adversely impacted. Consequently, h was taken to be $0.25{\cdot}H$.

For an axial flow pump, the guide vane inlet angle (β_0) can be determined based on the design condition, the guide vane inlet angle being consistent with the direction of the flow absolute velocity at the impeller outlet based on the design discharge condition (**Figure 4A**), the stream flowing into the guide vane smoothly. When the pump operates in an off-design condition, the inlet angle does not match the flow direction (**Figures 4B,C**), flow impact and separation being generated in the guide vane, increasing the hydraulic loss and reducing efficiency. In **Figure 4**, v_0, v_s, v_L are the absolute velocity of the flow at impeller outlet under the design condition, smaller discharge condition, and larger discharge condition, respectively; w_0, w_s, w_L are the relative velocity of the flow at impeller outlet under the design condition, smaller discharge condition, and larger discharge condition, respectively; u is the transport velocity; α_0, α_s, α_L are the angle between absolute velocity and transport velocity under the design condition, smaller discharge condition, and larger discharge condition, respectively.

The guide vane inlet angle (β_0) can be determined based on the design working conditions. For ease of expression, the inlet angle adjustment ($\Delta\beta$) can be taken to be 0° when the guide vane inlet angle is β_0, as shown in **Figure 5A**. To improve the efficiency under the larger discharge condition, based on the flow direction at the impeller outlet, the guide vane inlet angle should be rotated clockwise based on β_0, as shown in **Figure 5B** so that the stream can flow smoothly into the guide vane. For the vertical axial flow pump of the pumping station, the inlet angle adjustment (u) can be taken to be −12°.

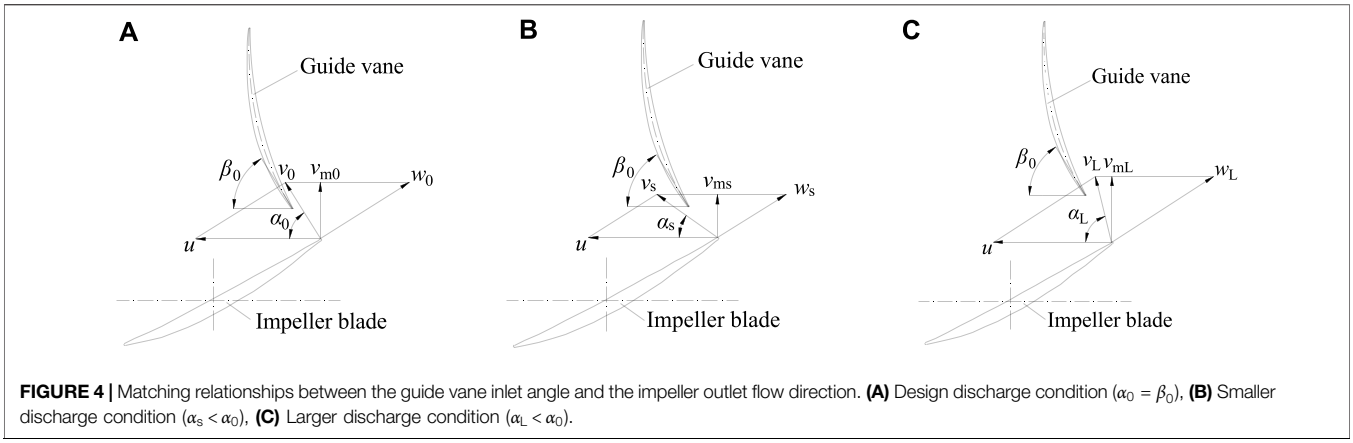

FIGURE 4 | Matching relationships between the guide vane inlet angle and the impeller outlet flow direction. **(A)** Design discharge condition ($\alpha_0 = \beta_0$), **(B)** Smaller discharge condition ($\alpha_s < \alpha_0$), **(C)** Larger discharge condition ($\alpha_L < \alpha_0$).

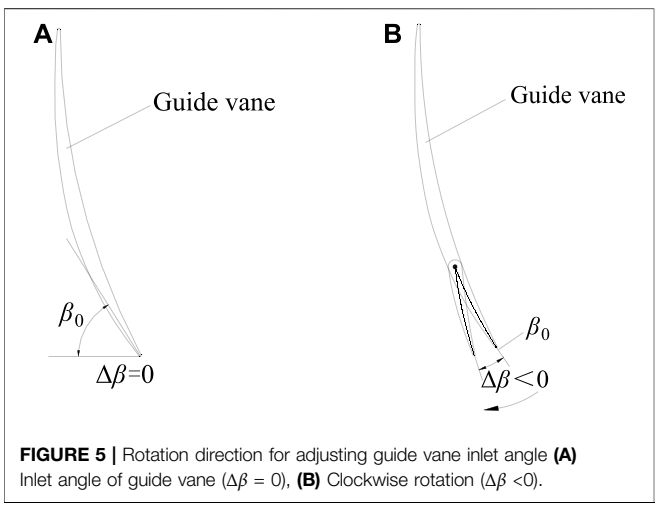

FIGURE 5 | Rotation direction for adjusting guide vane inlet angle **(A)** Inlet angle of guide vane ($\Delta\beta = 0$), **(B)** Clockwise rotation ($\Delta\beta < 0$).

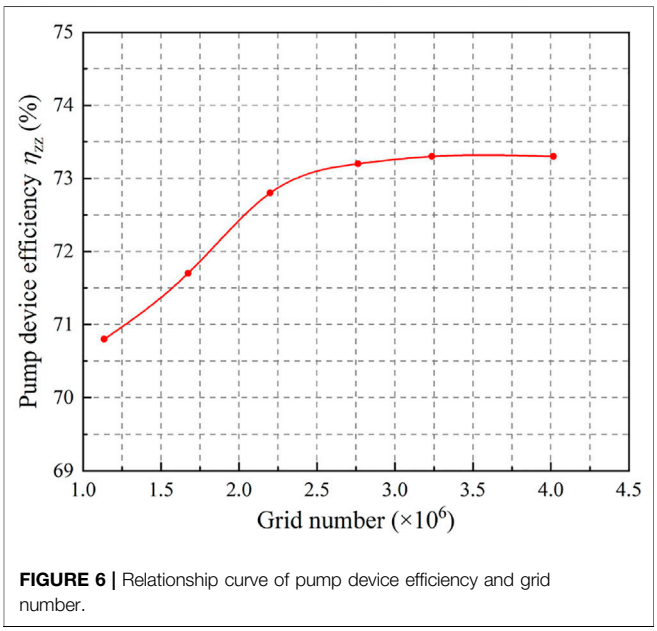

FIGURE 6 | Relationship curve of pump device efficiency and grid number.

Numerical Simulation Method

Governing Equations and Turbulence Model

The Reynolds-averaged Navier-Stokes equations can be applied to solve the flow field in a vertical axial flow pump device, as follows:

$$\frac{\partial \rho}{\partial t} + \rho \frac{\partial \overline{u_i}}{\partial x_i} = 0 \tag{1}$$

$$\rho \frac{\partial \overline{u_i}}{\partial t} + \rho \frac{\partial \overline{u_i}\,\overline{u_j}}{\partial x_j} = -\frac{\partial \bar{p}}{\partial x_i} + \frac{\partial}{\partial x_j}\left[\mu\left(\frac{\partial \overline{u_i}}{\partial x_j} + \frac{\partial \overline{u_j}}{\partial x_i}\right) - \rho \overline{u_i' u_j'}\right] + F_i \tag{2}$$

where ρ is the density, t is time, $\overline{u_i}$ and $\overline{u_j}$ are the mean velocity components, $\bar{p}$ is the mean pressure, x_i and x_j are coordinate directions, μ is the dynamic viscosity, F_i is the body force component, $\rho \overline{u_i' u_j'}$ is the Reynolds stress, and u_i' and u_j' are fluctuating velocity components, respectively.

There are many turbulence models for fluid flow simulations (Li et al., 2020; Kan et al., 2021b; Han et al., 2021). The Renormalization Group (RNG) $k-\varepsilon$ turbulence model was chosen to solve the flow in the pump device, because this model is suitable for solving rotating, separated, and vortex flows (Jafarzadeh et al., 2011; Qiao et al., 2018; Jiao et al., 2019; Caruso amd Meskell, 2021). The k and ε equations of the RNG $k-\varepsilon$ turbulence model can be expressed as follows:

$$\rho \frac{\partial k}{\partial t} + \rho \frac{\partial k \overline{u_i}}{\partial x_i} = \frac{\partial}{\partial x_j}\left[\left(\mu + \frac{\mu_t}{\sigma_k}\right)\frac{\partial k}{\partial x_j}\right] + G_k - \rho\varepsilon \tag{3}$$

$$\rho \frac{\partial \varepsilon}{\partial t} + \rho \frac{\partial \varepsilon \overline{u_i}}{\partial x_i} = \frac{\partial}{\partial x_j}\left[\left(\mu + \frac{\mu_t}{\sigma_\varepsilon}\right)\frac{\partial \varepsilon}{\partial x_j}\right] + \frac{C_{1\varepsilon}}{k} G_k - C_{2\varepsilon}\rho\frac{\varepsilon^2}{k} \tag{4}$$

where G_k is the turbulence kinetic energy production term, $C_{1\varepsilon}$ is an empirical constant, $C_{2\varepsilon}$ is an empirical constant, σ_k is the corresponding Prandtl number for the turbulence kinetic energy k, and σ_ε is the corresponding Prandtl number for the turbulence kinetic energy dissipation rate ε.

Computational Domain and Mesh Generation

The computational domain of the three-dimensional turbulence flow simulations for the pump device comprises the forebay, inlet conduit, impeller, guide vane, outlet conduit, and outlet sump. The bodies of the inlet conduit, impeller, guide vane, and

TABLE 1 | Grid number of each component of the computational domain of the pump device.

Component of computational domain	Forebay	Inlet conduit	Impeller	Guide vane	Outlet conduit	Outlet sump
Grid number ($\times 10^4$)	33.2	53.2	57.9	91.5	55.9	32.3

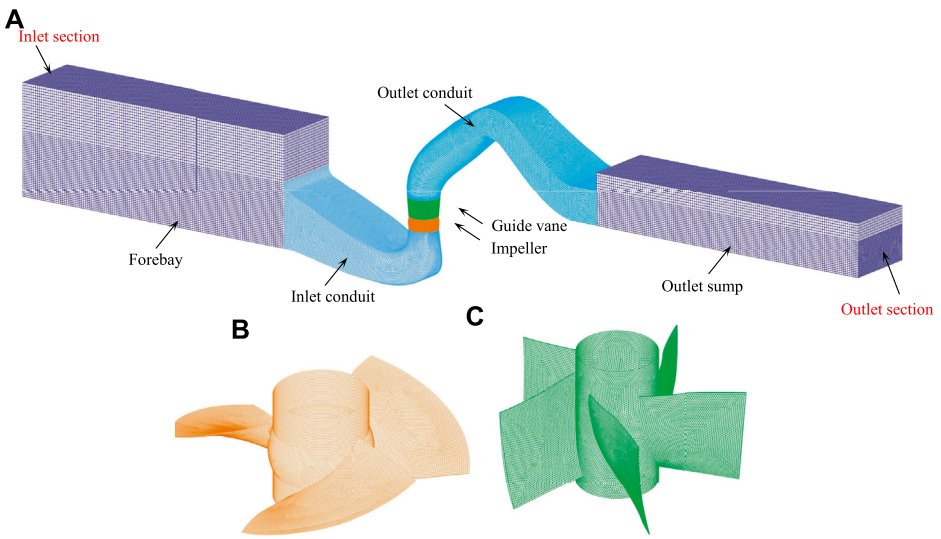

FIGURE 7 | Computational domains and mesh generations of vertical axial flow pump device. **(A)** Pump device, **(B)** Impeller, **(C)** Guide vane.

outlet conduit and the fluid flow within them are complex; thus, an unstructured mesh was adopted. The bodies and fluid flow of the forebay and outlet sump are, however, simple; therefore, a structured mesh was adopted. To obtain the most economical grid number, the grid independence was checked. **Figure 6** shows the relationship between the pump device efficiency and grid number under the conditions of a blade angle of 0°, guide vane inlet angle adjustment of 0°, and discharge of 245 L/s. When the gird number exceeds approximately 3,240,000, the pump efficiency changes slightly. Consequently, the number of mesh cells for the vertical axial flow pump device was chosen to be 3,240,000, the grid numbers of each component being listed in **Table 1**. The value of $y+$ affects the calculation accuracy: in this calculation the $y+$ value of the impeller wall was 14.8. The computational domains and mesh generations for them are shown in **Figure 7**.

Boundary Conditions and Numerical Settings

The inlet boundary was set in the forebay, the velocity being uniformly distributed on the inlet boundary, and the flow direction being perpendicular to it. Because the discharge was known, the velocity inlet boundary condition was adopted. The outlet boundary was set at the outlet sump, far from the outlet section of the outlet conduit. The flow direction was perpendicular to the outlet boundary, the flow being fully developed there so that the outflow boundary condition could be adopted there. The bottom of the forebay and outlet sump, the side walls of the conduit, the surface of the guide vane, and the surface of the impeller blade were solid walls, the impeller blade surfaces being set as a rotation wall. The surfaces of the forebay and outlet sump were free water surfaces, the symmetry boundary being specified on the water surface.

In the numerical simulations, the SIMPLEC algorithm was used to solve the pressure-velocity coupling equations, the first-order upwind differencing scheme was used to solve the governing equations, k and ε , and the convergence precision was set to 1×10^{-7}.

The numerical simulation conditions were as follows: the model pump impeller diameter (D_m) and rotation speed (n_m) were 300 mm and 1,200 r/min, respectively; the impeller blade angles (α) were −4°, −2°, and 0°; and the guide vane inlet angle adjustments ($\Delta\beta$) were 0° and −12°. **Figure 8** shows a perspective view of the vertical axial flow pump with two guide vane inlet angle adjustments.

Model Test Method

The model vertical axial flow pump device included all flow conduits, the model inlet and outlet conduits being made of steel plates. An image of the model vertical axial flow pump device installed on the pumping station test bench at Yangzhou University is shown in **Figure 9**. The uncertainty of the pump device efficiency test in this experimental study was ±0.36%, the main test instruments of the test bench being listed in **Table 2**. Consistent with the numerical calculations, the energy

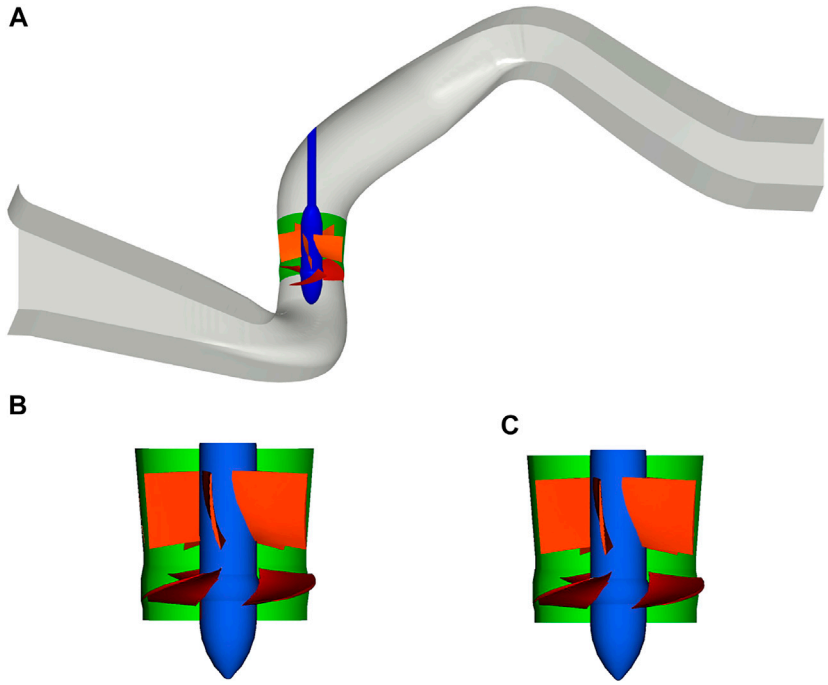

FIGURE 8 | Perspective view of the model vertical axial flow pump device. **(A)** Pump Device, **(B)** Pump Segment ($\Delta\beta = 0^{\circ}$), **(C)** Pump Segment ($\Delta\beta = -12^{\circ}$)

FIGURE 9 | Image of vertical axial flow pump device model.

TABLE 2 | Main test instruments of test bench.

Measuring items	Instrument	Instrument model	Accuracy
Head	Differential pressure transmitter	EJA110A	±0.1%
Flow rate	Electromagnetic flowmeter	E-mag	±0.2%
Torque and rotation speed	Torque and speed sensor	JC1A-500	±0.1%

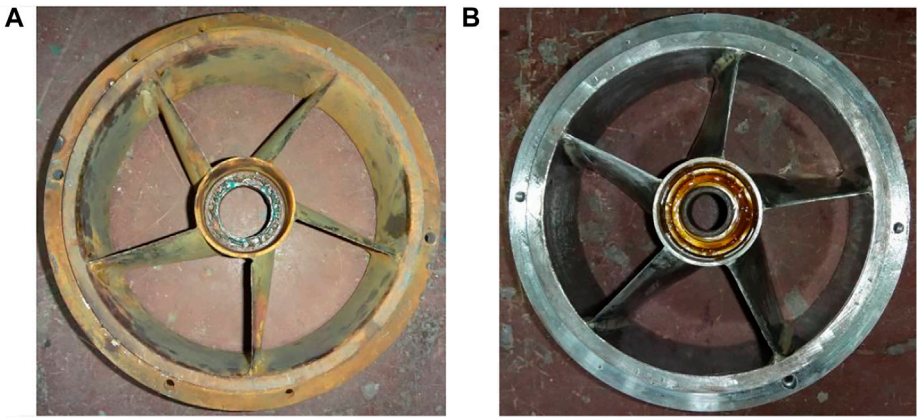

FIGURE 10 | Images of model guide vanes with inlet angle adjustments $\Delta\beta$ of 0° and −12°, respectively. **(A)** $\Delta\beta$ = 0°, **(B)** $\Delta\beta$ = −12°.

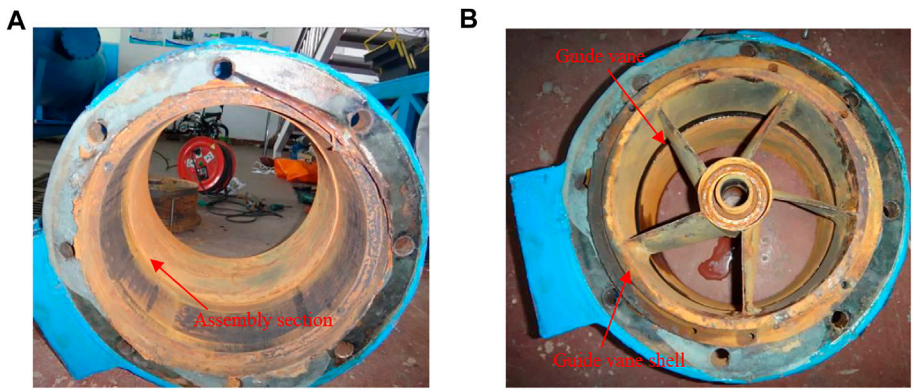

FIGURE 11 | Images of the model guide vane assembly. **(A)** Guide vane shell, **(B)** Assembled guide vane.

performance test of the pump devices with inlet angle adjustments ($\Delta\beta$) of 0° and −12° was conducted under 3 impeller blade angles (α) of −4°, −2°, and 0°, respectively. The head, torque, and rotation speed of the pump device are measured at different flow discharges under each impeller blade angle and inlet angle adjustment of guide vane, and the pump device efficiency is calculated according to the test results. The flow discharge change is regulated by valve.

The impeller blade angle was changed by adjusting the blade angle, while the guide vane inlet angle was changed by using two model guide vanes. The guide vane with an inlet angle adjustment ($\Delta\beta$) of 0° was the original guide vane of the TJ04-ZL-07 pump model, as shown in **Figure 10A**. The guide vane with an inlet angle adjustment ($\Delta\beta$) of −12° was constructed, as shown in **Figure 10B**. The model guide vane was divided into two parts—that is, the guide vane shell and the guide vane itself, the guide vane shell being shown in **Figure 11A**. The two model guide vanes had the same shell; thus, the energy performance of the pump device with two guide vane inlet angles could be tested and compared simply by replacing the guide vane. The assembly of the guide vane and guide vane shell is shown in **Figure 11B**.

RESULTS AND ANALYSIS

Numerical Simulation Results and Analysis

Under the conditions of the impeller blade angles (α) of −4°, −2°, and 0°, respectively, three-dimensional turbulence flow in the vertical axial flow pump device was calculated when the inlet angle adjustments of the guide vane ($\Delta\beta$) were 0° and −12°, respectively. Based on the calculation results, the $Q \sim H_{zz}$ and $Q \sim \eta_{zz}$ relationship curves of the vertical axial flow pump device are shown in **Figure 12**.

From **Figure 10**, it can be seen that there is an intersection point (O) between the two $Q \sim \eta_{zz}$ curves with inlet angle adjustments ($\Delta\beta$) of 0° and −12°, respectively. On the left side of point O, the pump device efficiency (η_{zz}) at an inlet angle adjustment ($\Delta\beta$) of 0° is higher than that at an inlet angle adjustment ($\Delta\beta$) of −12°; on the right side of point O, the pump device efficiency (η_{zz}) at an inlet angle adjustment ($\Delta\beta$)

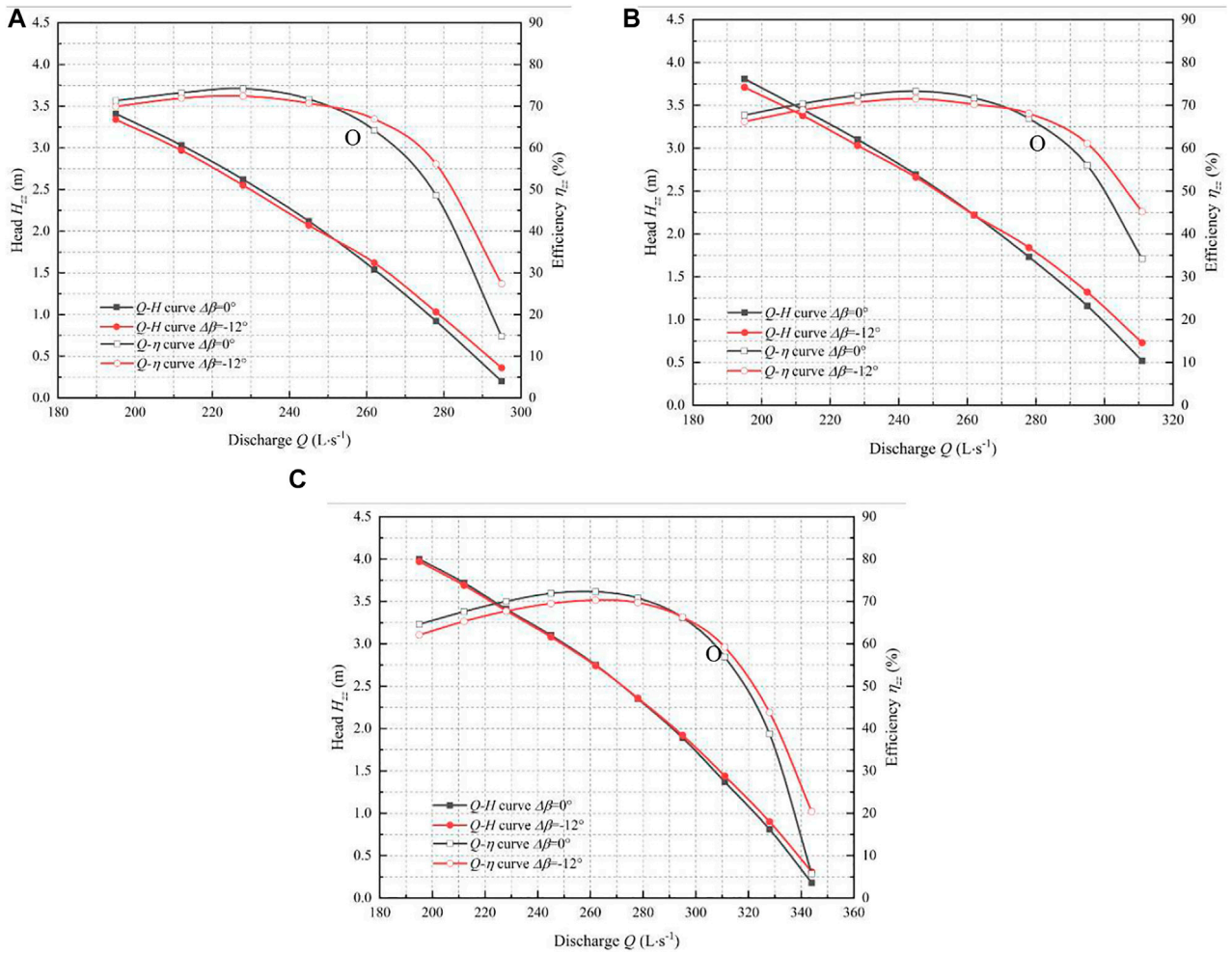

FIGURE 12 | Numerical calculation results of $Q \sim H_{zz}$ and $Q \sim \eta_{zz}$ relationship curves of the axial flow pump device with $\Delta\beta$ of 0° and −12°, respectively. **(A)** $\alpha = -4°$, **(B)** $\alpha = -2°$, **(C)** $\alpha = 0°$.

of 0° is lower than that at an inlet angle adjustment ($\Delta\beta$) of −12°. That is, the farther away from point O one gets, the larger the difference between the efficiency of the two pump devices. Compared with the pump device with an inlet angle adjustment ($\Delta\beta$) of 0°, the optimal efficiency of the pump device with an inlet angle adjustment ($\Delta\beta$) of −12° is reduced by approximately 2%.

To analyze the influence of the guide vane inlet angle adjustment, based on the composition of the pump, the relationship between the pump device efficiency (η_{zz}), impeller efficiency (H_{yl}), vane efficiency (η_{dy}), and conduit efficiency (η_{ld}) can be expressed as follows:

$$\eta_{zz} = \frac{\rho g Q H_{zz}}{P_{bz}} = \frac{\rho g Q H_{bd}}{P_{bz}} \times \frac{H_{zz}}{H_{bd}} = \eta_{bd} \times \eta_{ld} = \eta_{yl} \times \eta_{dy} \times \eta_{ld} \tag{5}$$

where η_{zz} is the pump device efficiency, g is the acceleration of gravity, Q is the discharge, H_{zz} is the pump head, P_{bz} is the pump shaft power, η_{bd} is the pump segment efficiency, η_{yl} is the impeller efficiency, and H_{yl} is the impeller head.

The pump segment efficiency (η_{bd}), impeller efficiency (η_{yl}), guide vane efficiency (η_{dy}), and conduit efficiency (η_{ld}) can be expressed as follows:

$$\eta_{bd} = \frac{\rho g Q H_{bd}}{P_{bz}} \times 100\% \tag{6}$$

$$\eta_{yl} = \frac{\rho g Q H_{yl}}{P_{bz}} \times 100\% \tag{7}$$

$$\eta_{dy} = \frac{\rho g Q H_{bd}}{\rho g Q H_{yl}} = \frac{H_{bd}}{H_{yl}} = \frac{H_{yl} - \Delta h_{dy}}{H_{yl}} \times 100\% \tag{8}$$

$$\eta_{ld} = \frac{\rho g Q H_{zz}}{\rho g Q H_{bd}} = \frac{H_{zz}}{H_{bd}} = \frac{H_{zz}}{H_{zz} + \Delta h_{ld}} \times 100\% \tag{9}$$

where H_{bd} is the pump segment head, H_{yl} is the impeller head, Δh_{dy} is the guide vane hydraulic loss, and Δh_{ld} is the conduit hydraulic loss.

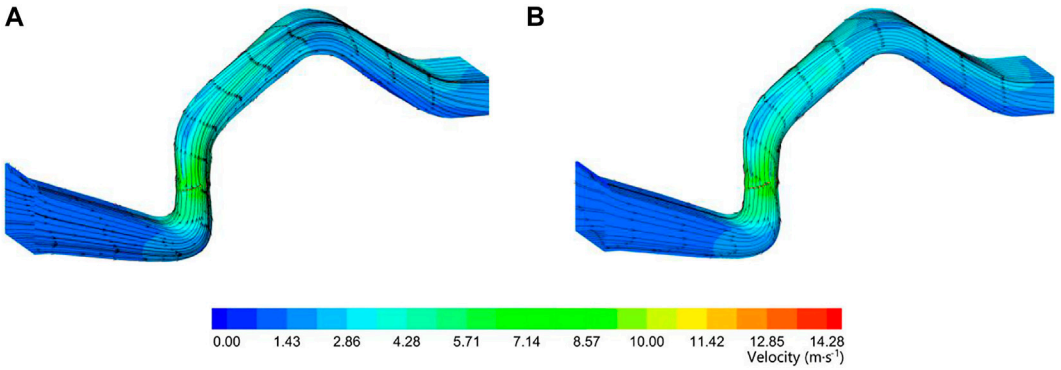

FIGURE 13 | Pump device flow fields with $\Delta\beta$ of 0° and −12°, respectively. **(A)** $\Delta\beta$ = 0°, **(B)** $\Delta\beta$ = −12°.

TABLE 3 | Comparison of energy performance parameters of pump devices with $\Delta\beta$ of 0° and −12°.

$\Delta\beta$ (°)	H_{yl} (m)	η_{yl} (%)	H_{bd} (m)	Δh_{dy} (m)	η_{dy} (%)	η_{bd} (%)	Δh_{ld} (m)	H_{zz} (m)	η_{ld} (%)	η_{zz} (%)
0	1.625	77.1	1.414	0.211	87.0	67.1	0.603	0.811	57.4	38.5
−12	1.634	77.3	1.496	0.138	91.6	70.8	0.596	0.900	60.2	42.6

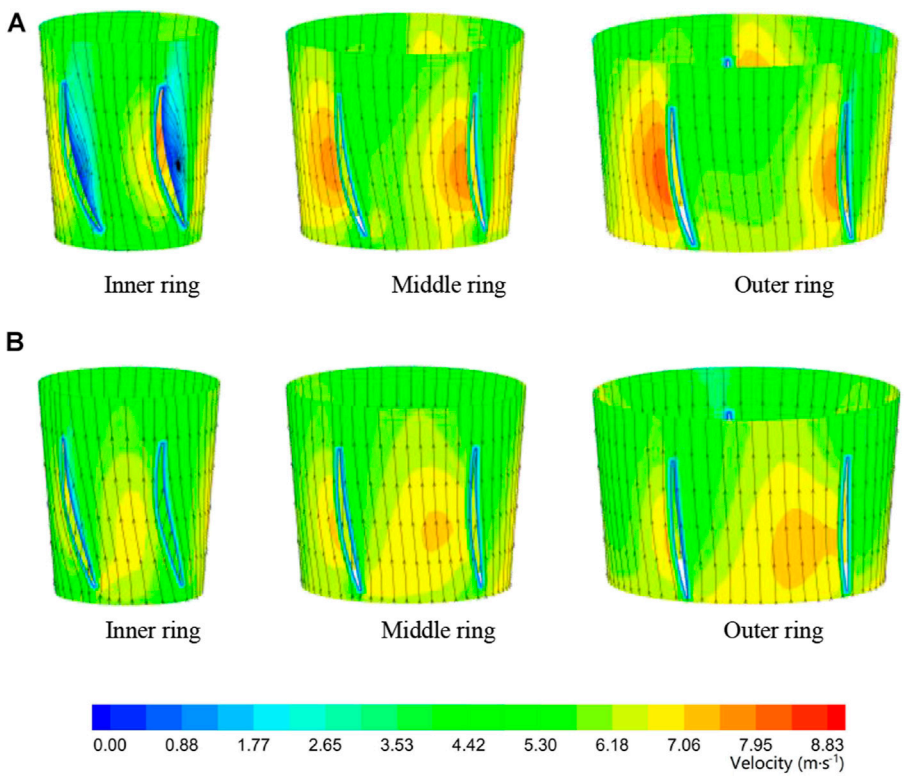

FIGURE 14 | Guide vane flow fields with $\Delta\beta$ of 0° and −12°, respectively. **(A)** $\Delta\beta$ = 0°, **(B)** $\Delta\beta$ = −12°.

The three-dimensional turbulence flow in the pump device with a guide vane inlet angle adjustment ($\Delta\beta$) of 0° and −12° were simulated when the impeller blade angle (α) was 0° and the discharge (Q) was 0.33 m^3/s, the flow fields of the two pumps being shown in **Figure 13**. It can be seen that the flow fields in the conduits of the pump device are the same when the inlet angles of

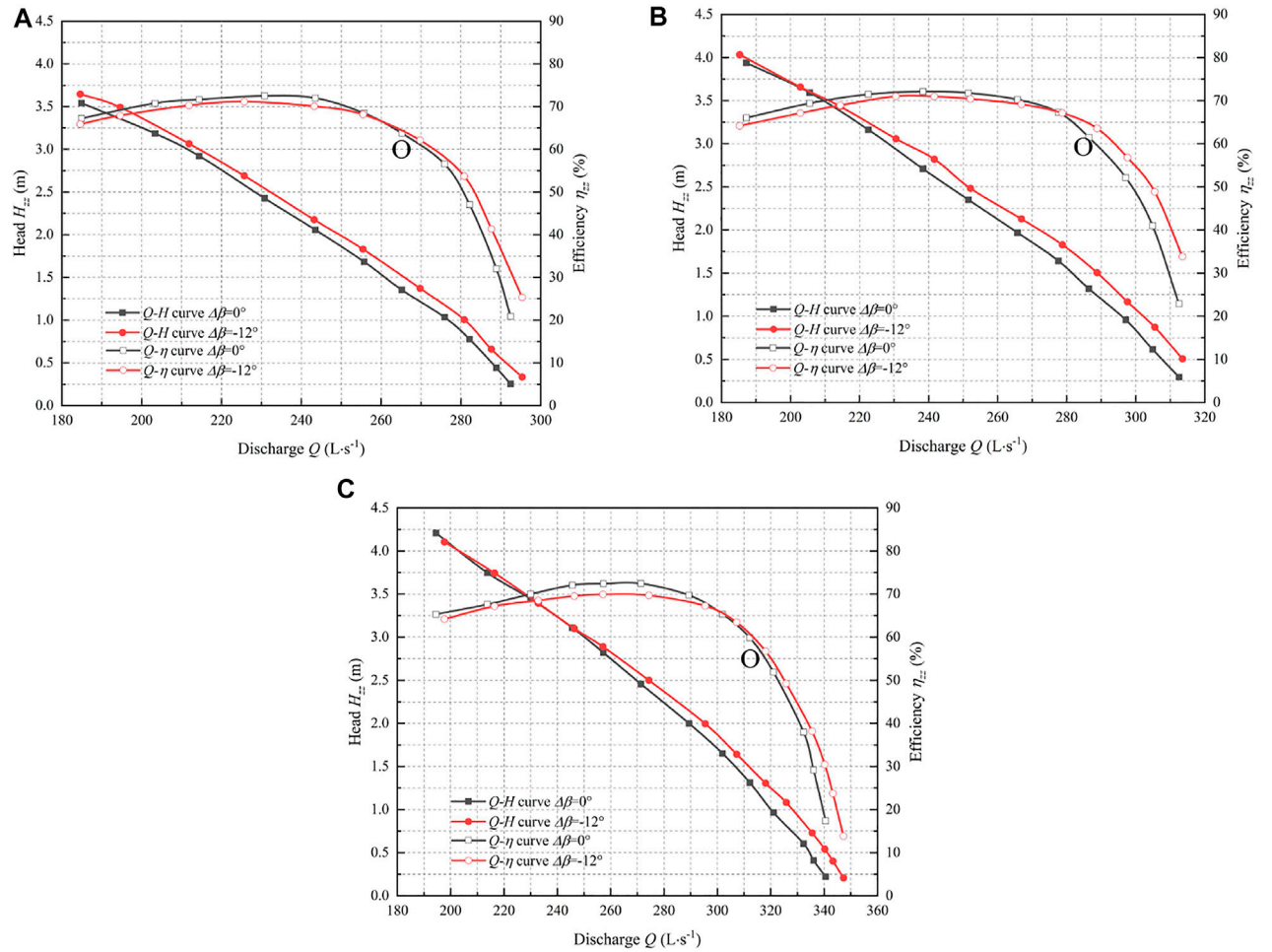

FIGURE 15 | Model test results of $Q \sim H_{zz}$ and $Q \sim \eta_{zz}$ relationship curves of the axial flow pump device with $\Delta\beta$ of 0° and −12°, respectively. **(A)** $\alpha = -4°$, **(B)** $\alpha = -2°$, **(C)** $\alpha = 0°$.

the guide vane differ, the flow velocity of the water in the inlet conduit gradually increases, the flow decreases smoothly and evenly, and the water flow in the outlet conduit diffuses smoothly without poor flow patterns. Based on the calculated hydraulic loss of each part, the relationships between Δh_{dy} and η_{dy}, η_{bd}, and η_{zz} were analyzed, and the influence of $\Delta\beta$ on the vertical axial flow pump device efficiency was examined. The main energy performance parameters of the pump device with inlet angle adjustments ($\Delta\beta$) of 0° and −12° under the chosen working conditions are listed in **Table 3**.

It can be seen that when $\Delta\beta$ is adjusted from 0° to −12° for the vertical axial flow pump device, the impeller heads (H_{yl}) and impeller efficiencies (η_{yl}) are the same, the conduit hydraulic losses (Δh_{ld}) change a little, and the conduit flow fields remain the same. However, the guide vane hydraulic loss (Δh_{dy}) decreases from 0.211 to 0.138 m; thus, the guide vane efficiency (η_{dy}) increases from 87.0 to 91.6%, the pump segment efficiency (η_{bd}) increases from 67.1 to 70.8%, and the pump device efficiency increases from 38.5 to 42.6%.

Under the conditions of an impeller angle of 0° and a discharge of 0.33 m^3/s, the flow fields of the outer, middle, and inner rings of the guide vane when $\Delta\beta$ is 0° are shown in **Figure 14A**, the flow fields when $\Delta\beta$ is −12° being shown in **Figure 14B**. It can be seen that when $\Delta\beta$ is 0°, the direction of water flow entering the guide vane does not match the guide vane inlet angle; therefore, the separation flow and vortex are at the front of the guide vane, as shown in **Figure 14A**. Conversely, when $\Delta\beta$ is −12°, the direction of water flow entering the guide vane matches the guide vane inlet angle. Thus, there is no vortex in the guide vane, as shown in **Figure 14B**, and the guide vane hydraulic loss decreases.

Model Test Results and Analysis

A model test for the vertical axial flow pump device was conducted to verify the numerical computational results. Based on the test results, the $Q \sim H_{zz}$ and $Q \sim \eta_{zz}$ curves of the model pump device with inlet angle adjustments ($\Delta\beta$) of 0° and −12°, respectively, under different impeller blade angles are shown in **Figure 15**. The energy performance parameters of the main working conditions for the model vertical axial flow pump device with $\Delta\beta$ of 0° and −12° are listed in **Table 4**.

From the pump device model test results, it can be concluded that

TABLE 4 | Comparison of performance parameters at main operating points of the pump devices.

α (°)	$\Delta\beta$ (°)	Optimal operating point of the pump			Intersection point O of Q ~ H_{zz} curve	
		Q (L/s)	H_{zz} (m)	η_{zz} (%)	Q (L/s)	η_{zz} (%)
−4	0	230.8	2.43	72.5	258.6	67.5
	−12	225.7	2.69	71.1		
−2	0	238.4	2.71	72.1	278.7	67.1
	−12	230.5	3.06	71.0		
0	0	271.4	2.46	72.4	301.9	65.3
	−12	257.1	2.89	69.9		

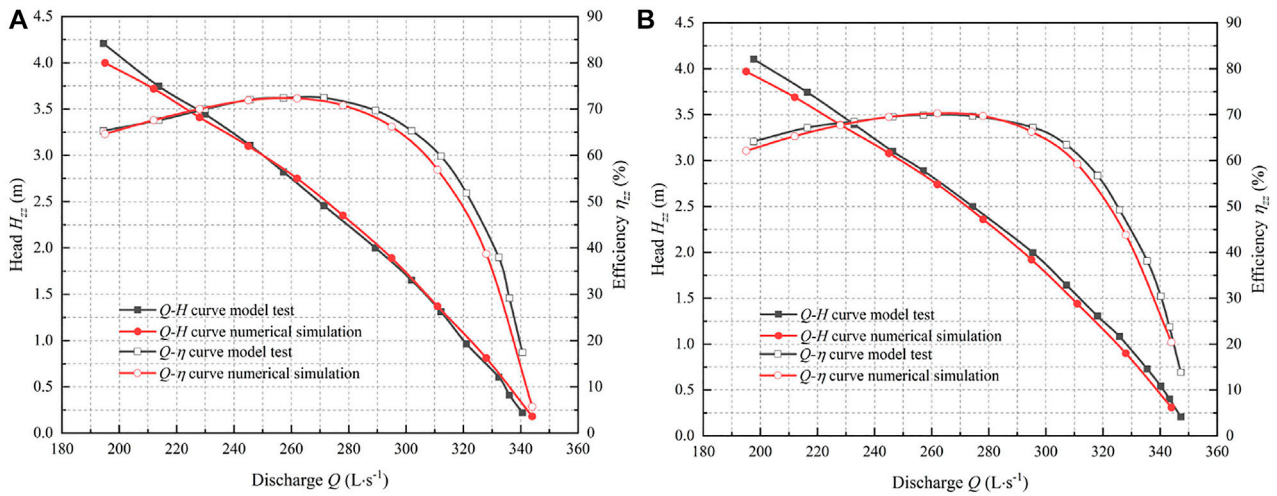

FIGURE 16 | Comparison of model test and numerical calculation results of energy performance of the pump device with α of 0°. **(A)** $\Delta\beta$ = 0°, **(B)** $\Delta\beta$ = −12°.

1) There is an intersection point O between the two $Q \sim \eta_{zz}$ curves of the pump device with two inlet angle adjustments of 0° and −12°. The discharge and pump device efficiency are 258.6 L/s and 67.5%, respectively, when the impeller blade angle is −4°, the discharge and pump device efficiency are 278.7 L/s and 67.1%, respectively, when the impeller blade angle is −2°, and the flow discharge and pump device efficiency are 301.9 L/s and 65.3%, respectively, when the impeller blade angle (α) is 0°.
2) When $\Delta\beta$ is adjusted from 0° to −12°, the pump device efficiency is reduced. For the pump impeller blade angles of −4°, −2°, and 0°, the pump device efficiency decreases by 1.4, 1.1, and 2.5%, respectively.
3) When $\Delta\beta$ is adjusted from 0° to −12°, in the large-discharge area—which is on the right-hand side of point O—the pump device efficiency with a $\Delta\beta$ of −12° is higher than with a $\Delta\beta$ of 0°. Consequently, the lower the head and the greater the discharge, the greater the difference in pump efficiency.

A comparison between the numerical simulation and model test results of the pump device energy performance with an impeller blade angle (α) of 0° is shown in **Figure 16**. The maximum difference in the pump device efficiency (between numerical simulation and model test results) is approximately 3%, the maximum difference of the pump device head being approximately 0.2 m. In short, the numerical calculations are consistent with the model test results.

CONCLUSION

1) The guide vane inlet angle had a significant impact on the energy performance of vertical axial flow pump device. When the guide vane inlet angle was adjusted in a clockwise direction, the pump device efficiency was reduced at the pump device optimal operating point, but its efficiency improved in low-head and large-discharge areas.
2) When the guide vane inlet angle did not match the direction of flow from the impeller outlet in the axial flow pump device, flow separation and a vortex were generated in the guide vane. By adjusting the guide vane inlet angle, the flow field could be significantly improved, the hydraulic loss of guide vane decreasing, and the energy performance of the axial flow pump device improving.
3) When the operating conditions of the low-head pump device are frequently in the large-discharge and low-head areas that deviate from the high-efficiency area due to limitations of the pump model or motor itself, these research results could be used to improve the energy performance of pump device in the low-head area.

DATA AVAILABILITY STATEMENT

The raw data supporting the conclusions of this article will be made available by the authors, without undue reservation.

AUTHOR CONTRIBUTIONS

LX, analysis, writing and revision; HZ, methodology and revision; CW, analysis and revision; DJ and WS, validation and revision; and WL and LL, data analysis and revision.

FUNDING

This work was supported by the National Natural Science Foundation of China (Grant No. 51309200, Grant No. 51779215), the High-tech Key Laboratory of Agricultural Equipment and Intelligentization of Jiangsu Province, Key Laboratory of Modern Agricultural Equipment and Technology (Jiangsu University), the Ministry of Education (NZ201604), and the Jiangsu South-to-North Water Diversion Technology R and D Project (JSNSBD202105).

REFERENCES

Al-Obaidi, A. R. (2021). Analysis of the Effect of Various Impeller Blade Angles on Characteristic of the Axial Pump with Pressure Fluctuations Based on Time- and Frequency-Domain Investigations. *Iran J. Sci. Technol. Trans. Mech. Eng.* 45, 441–459. doi:10.1007/s40997-020-00392-3

Caruso, F., and Meskell, C. (2021). Effect of the Axial gap on the Energy Consumption of a Single-Blade Wastewater Pump. *Proc. Inst. Mech. Eng. A: J. Power Energ.* 235, 432–439. doi:10.1177/0957650920927366

Feng, J., Zheng, Y., and Luo, X. (2012). Effects of Exit Guide Vane on Performance of Axial-Flow Pump Device. *Water Resour. Power* 30, 126–128. doi:10.3969/j.issn.1000-7709.2012.08.037

González, J., and Santolaria, C. (2006). Unsteady Flow Structure and Global Variables in a Centrifugal Pump. *J. Fluids Eng. Trans. ASME.* 128, 937–946. doi:10.1115/1.2234782

Han, Y., Zhou, L., Bai, L., Shi, W., and Agarwal, R. (2021). Comparison and Validation of Various Turbulence Models for U-bend Flow with a Magnetic Resonance Velocimetry experiment. *Phys. Fluids* 33. doi:10.1063/5.0073910

Hu, J., Huang, S., and Wang, P. (2008). Research on Hydrodynamic Characteristics of Axial Waterjet Pump with Guide Vane. *J. Hydroelectr. Eng.* 27, 32–36. doi:10.3969/j.issn.1003-1243.2008.01.007

Jafarzadeh, B., Hajari, A., Alishahi, M. M., and Akbari, M. H. (2011). The Flow Simulation of a Low-Specific-Speed High-Speed Centrifugal Pump. *Appl. Math. Model.* 35, 242–249. doi:10.1016/j.apm.2010.05.021

Jiao, W., Cheng, L., Xu, J., and Wang, C. (2019). Numerical Analysis of Two-phase Flow in the Cavitation Process of a Waterjet Propulsion Pump System. *Processes* 7, 690. doi:10.3390/pr7100690

Kan, K., Chen, H., Zheng, Y., Zhou, D., Binama, M., and Dai, J. (2021a). Transient Characteristics during Power-Off Process in a Shaft Extension Tubular Pump by Using a Suitable Numerical Model. *Renew. Energ.* 164, 109–121. doi:10.1016/j.renene.2020.09.001

Kan, K., Yang, Z., Lyu, P., Zheng, Y., and Shen, L. (2021b). Numerical Study of Turbulent Flow Past a Rotating Axial-Flow Pump Based on a Level-Set Immersed Boundary Method. *Renew. Energ.* 168, 960–971. doi:10.1016/j.renene.2020.12.103

Kan, K., Zheng, Y., Fu, S., Liu, H., Yang, C., and Zhang, X. (2017). Dynamic Stress of Impeller Blade of Shaft Extension Tubular Pump Device Based on Bidirectional Fluid-Structure Interaction. *J. Mech. Sci. Technol.* 31, 1561–1568. doi:10.1007/s12206-017-0303-1

Li, X., Shen, T., Li, P., Guo, X., and Zhu, Z. (2020). Extended Compressible thermal Cavitation Model for the Numerical Simulation of Cryogenic Cavitating Flow. *Int. J. Hydrogen Energ.* 45, 10104–10118. doi:10.1016/j.ijhydene.2020.01.192

Li, Z., Yang, M., and Wang, X. (2009). Experimental Study of Guide Vane Influence on Performance of Axial-Flow Pump. *Drain. Irrig. Mach.* 27, 15–18.

Liu, J., Gong, Y., and Wang, Y. (2008). Influence of Pump Diameter on Hydraulic Loss of Vertical Pump Device. S. North Water Transfers Water Sci. *Technol.* 6, 67–69. doi:10.13476/j.cnki.nsbdqk.2008.05.026

Liu, N., Wang, Y. S., and Zhang, G. (2006). *Model Pump Test on the Same Test-Bed for the South-To-North Water Diversion.* Beijing, China: China Water Power Press.

Patil, A., Sundar, S., Delgado, A., and Gamboa, J. (2019). CFD Based Evaluation of Conventional Electrical Submersible Pump for High-Speed Application. *J. Petrol. Sci. Eng.* 182. doi:10.1016/j.petrol.2019.106287

Qi, L., Zhang, Y., and Zhang, G. (2017). Model Test and Analysis of Pump Device of Miyun Reservoir Regulation and Storage Project of Incoming Water from South-To-North Transfer Project. *Yellow River* 6, 133–137. doi:10.3969/j.issn.1000-1379.2017.06.031

Qian, J., Gao, Z., Liu, B., and Jin, Z. (2018). Parametric Study on Fluid Dynamics of Pilot-Control Angle globe Valve. *J. Fluids Eng.* 140. doi:10.1115/1.4040037

Qian, Z., Wang, F., Wang, Z., and Zhou, W. (2013). Experimental Study on Hydraulic Performance of Saddle Zone in Axial-Flow Pump with Adjustable Guide Vane. *J. Drain. Irrig. Mach. Eng.* 31, 461–465. doi:10.3969/j.issn.1674.8530.2013.06.001

Qian, Z., Wang, Y., Huai, W., and Lee, Y. (2010). Numerical Simulation of Water Flow in an Axial Flow Pump with Adjustable Guide Vanes. *J. Mech. Sci. Technol.* 24, 971–976. doi:10.1007/s12206-010-0212-z

Tang, F., and Wang, G. (2006). Influence of Outlet Guide Vanes upon Performances of Waterjet Axial-Flow Pump. *J. Ship Mech.* 6, 19–26. doi:10.3969/j.issn.2006.06.003

Tang, S., Zhu, Y., and Yuan, S. (2021). An Improved Convolutional Neural Network with an Adaptable Learning Rate towards Multi-Signal Fault Diagnosis of Hydraulic Piston Pump. *Adv. Eng. Inform.* 50. doi:10.1016/j.aei.2021.101406

Wang, H. L., Hu, Q. X., Yang, Y., and Wang, C. (2021). Performance Differences of Electrical Submersible Pump under Variable Speed Schemes. *Int. J. Simul. Model.* 20, 76–86. doi:10.2507/ijsimm20-1-544

Wang, H., Long, B., Wang, C., Han, C., and Li, L. (2020a). Effects of the Impeller Blade with a Slot Structure on the Centrifugal Pump Performance. *Energies* 13, 1628. doi:10.3390/en13071628

Wang, H., Qian, Z., Zhang, D., Wang, T., and Wang, C. (2020b). Numerical Study of the Normal Impinging Water Jet at Different Impinging Height, Based on Wray-Agarwal Turbulence Model. *Energies* 13, 1744. doi:10.3390/en13071744

Wu, H., Tian, Y., Liao, W., Liu, B., and Song, W. (2016). Pumping Device Performance Analysis Based on the Miyun Storage Project of Cascade Pumping Stations. *China Rural Water Hydropower.* 11, 178–182.

Yu, J., Chen, Y., Zhu, Y., Lv, B., and Sun, P. (2018). Study on Pump Type Selection for Extra-low Head Pumping Station with Large Difference between Average and Highest Heads. *Water Resour. Hydropower Eng.* 49, 68–76. doi:10.13928/j.cnki.wrahe.2018.05.011

Zawistowski, T., and Kleiber, M. (2017). Gap Flow Simulation Methods in High Pressure Variable Displacement Axial Piston Pumps. *Arch. Computat Methods Eng.* 24, 519–542. doi:10.1007/s11831-016-9180-5

Zhang, L., Li, Y., Zong, L., Duan, Z., and Hua, X. (2011). Type Selection and Hydraulic Optimization of Vertical Axial-Flow Pump Assembly in Changgou Pumping Station of the East Route of South-To-North Water Transfer Project. S. North Water Transfers Water Sci. *Technol* 9, 15–18. doi:10.3724/SP.J.1201.2011.05015

Zhang, L., Wang, C., Zhang, Y., Xiang, W., He, Z., and Shi, W. (2021). Numerical Study of Coupled Flow in Blocking Pulsed Jet Impinging on a Rotating wall. *J. Braz. Soc. Mech. Sci. Eng.* 43, 508. doi:10.1007/s40430-021-03212-0

Zhou, J., Zhao, M., Wang, C., and Gao, Z. (2021). Optimal Design of Diversion Piers of Lateral Intake Pumping Station Based on Orthogonal Test. *Shock and Vibration* 2021, 1–9. doi:10.1155/2021/6616456

Zhou, Y., and Xu, H. (2007). The Influence of Diffuser on the Function of the Axial-Flow Pump. *Water Conserv. Electr. Power Mach.* 29, 28–29. doi:10.3969/j.issn.1674-1951.2007.09.010

Zhu, Y., Li, G., Wang, R., Tang, S., Su, H., and Cao, K. (2021). Intelligent Fault Diagnosis of Hydraulic Piston Pump Combining Improved Lenet-5 and Pso Hyperparameter Optimization. *Appl. Acoust.* 183. doi:10.1016/j.apacoust.2021.108336

Conflict of Interest: Author WS is employed by Jiangsu Water Supply Co., Ltd. In the Eastern Route of the S-to-N Water Diversion Project.

The remaining authors declare that the research was conducted in the absence of any commercial or financial relationships that could be construed as a potential conflict of interest.

Publisher's Note: All claims expressed in this article are solely those of the authors and do not necessarily represent those of their affiliated organizations, or those of the publisher, the editors and the reviewers. Any product that may be evaluated in this article, or claim that may be made by its manufacturer, is not guaranteed or endorsed by the publisher.